ISBN: 978-3-95450-220-2 ISSN: 2673-5474 doi: 10.18429/JACoW-FEL2022-TUP71

SPECTRO-TEMPORAL PROPERTIES OF COHERENTLY EMITTED ULTRASHORT RADIATION PULSES AT DELTA *

A. Radha Krishnan†, B. Büsing, A. Held, S. Khan, C. Mai, Z. Usfoor, V. Vijayan
Center for Synchrotron Radiation (DELTA), TU Dortmund, Dortmund, Germany

Abstract

At the 1.5 GeV synchrotron light source DELTA operated by the TU Dortmund University, the short-pulse facility employs the seeding scheme coherent harmonic generation (CHG) to produce ultrashort pulses in the vacuum ultraviolet and terahertz regime. This is achieved via a laser-induced electron energy modulation and a subsequent microbunching in a dispersive section. The spectro-temporal properties of the CHG pulses as well as the coherently emitted terahertz radiation are influenced by the seed laser parameters and can be manipulated by varying the laser pulse shape and the strength of the dispersive section. CHG spectra for different parameter sets were recorded and compared with the results of numerical simulations to reconstruct the spectra. A convolutional neural network was employed to extract the spectral phase information of the seed laser from the recorded spectra. In addition, the shaping of the coherently emitted THz pulses by controlling the seed pulse spectral phase using a spatial light modulator was also demonstrated.

INTRODUCTION

Synchrotron radiation is proven vital for the study of properties of matter in a variety of experiments due to its characteristics such as high intensity, collimation and tunable wavelength. However, a lower limit to the achievable pulse duration is given by the electron bunch length which is usually in the order of several tens of picoseconds. These pulses lack the temporal resolution to probe the atomic processes taking place on the sub-picosecond scale. On the other hand, conventional mode-locked lasers can produce light pulses in the femtosecond regime but are in the visible and infrared wavelength range. Coherent harmonic generation (CHG) [1] is a technique that combines the advantages of these two radiation sources to produce coherent femtosecond light pulses of short wavelength.

CHG in storage rings is similar to the high-gain harmonic-generation (HGHG) seeding scheme used for free-electron lasers (FEL) but without the FEL gain [2–4]. As depicted in Fig. 1, CHG is based on a laser-electron interaction in an undulator that is tuned to the seed laser wavelength (modulator). The laser-electron interaction induces a sinusoidal modulation of the electron energy, which is then transformed into a density modulation (microbunches) via a dispersive section (chicane). These microbunches results in coherent emission in a subsequent undulator that is tuned to a target

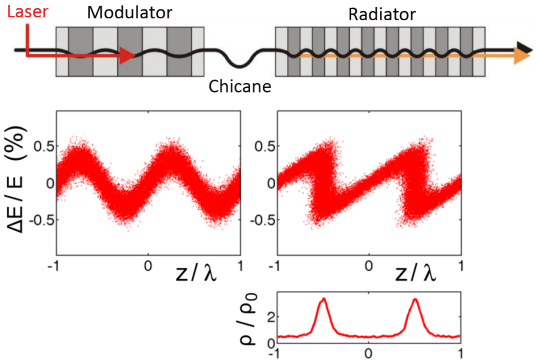

Figure 1: Magnetic setup for CHG, corresponding longitudinal phase space distributions and final longitudinal electron density.

harmonic of the seed laser wavelength (radiator). Since the laser pulse only modulates a very thin slice of the electron bunch, the resulting coherently emitted pulse will also have a pulse length comparable to that of the laser pulse.

The power of the CHG radiation at the n^{th} harmonic of the laser wavelength λ is given by

$$P(\lambda/n) \sim N_e^2 b_n^2 \tag{1}$$

where b_n is the bunching factor and N_e is the number of modulated electrons. For the CHG scheme, the bunching factor is given by [5],

$$b_n = |J_n(nAB)| e^{-\frac{n^2 B^2}{2}} \tag{2}$$

where $A = \Delta E_{\max}/\sigma_E$ is the relative energy modulation amplitude and $B = R_{56} k \sigma_E / E_0$ is the dimensionless chicane parameter. Here, R_{56} is the matrix element of the chicane describing its longitudinal dispersion which quantifies the strength of the chicane, E_0 is the nominal beam energy, σ_E is the rms energy spread and $k = 2\pi/\lambda$. When seeded with a Gaussian laser pulse, the energy modulation amplitude A varies longitudinally following the pulse shape of the laser. Since the amplitude of the energy modulation along the bunch is proportional to the electric field of the laser, the Gaussian distribution of the modulation follows a length larger than that of the seed pulse by a factor of $\sqrt{2}$. Due to this non-uniform energy modulation, the optimum R_{56} required will be different along the longitudinal position of the bunch. This allows one to manipulate the pulse shape of the CHG radiation by controlling the chicane strength. As can be seen in Fig. 2, the CHG radiation will be a single bell-shaped pulse for $R_{56} = 50$ µm (green line) where

* Work supported by BMBF (05K16PEA, 05K16PEB, 05K19PEB, 05K19PEC), DFG (INST 212/236-1 FUGG) and the federal state of NRW.
† arjun.krishnan@tu-dortmund.de

ISBN: 978-3-95450-220-2 ISSN: 2673-5474 doi: 10.18429/JACoW-FEL2022-TUP71

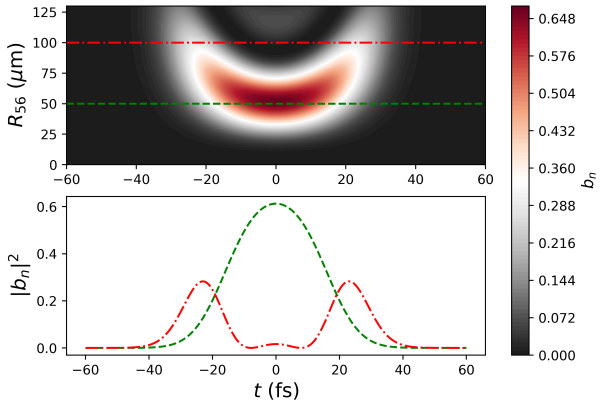

Figure 2: Intensity plot of theoretical bunching factor as a function of longitudinal position and chicane strength R_{56} (top). Bunching factor squared as a function of time along the specified lines in the top figure (bottom).

the bunching is maximized at the centre of the modulated slice. For stronger chicanes, e.g. 100 µm (red line), microbunching occurs for the electrons with a lower energy modulation at the head and tail of the slice, while the electrons at the centre with maximum energy modulation are overbunched. Consequently, this results in separate pulses originating from different longitudinal positions influencing the spectral properties of CHG radiation.

A laser pulse with central frequency ω_0 can be expressed in the frequency domain in terms of spectral amplitude $\tilde{E}(\omega)$ and spectral phase $\varphi(\omega)$

$$\tilde{E}(\omega) = |\tilde{E}_0(\omega)|e^{-i\varphi(\omega)}, \tag{3}$$

where $\varphi(\omega)$ can be expanded into a Taylor series as

$$\varphi(\omega) = D_0 + D_1 \cdot (\omega - \omega_0) + D_2 \cdot (\omega - \omega_0)^2 + D_3 \cdot (\omega - \omega_0)^3 + \ldots . \tag{4}$$

Here, D_0 is the central phase advance, D_1 is the group delay, D_2 is the group delay dispersion (GDD), and D_3 is the third order dispersion (TOD). A transform-limited pulse with shortest pulse length corresponds to a GDD of zero, while a non-zero GDD introduces a linear frequency chirp to the laser pulse. If the seed pulse is not chirped, the successive CHG pulses at high R_{56} have the same frequency, which results in interference fringes in the CHG spectra as shown in Fig. 3 (left). Instead, if the seed pulse has strong frequency chirp, the successive maxima of the bunching factor would result in maxima at specific frequencies in the CHG spectra, see Fig. 3 (right). In addition to the effects of GDD, a non-zero TOD in the seed pulse would influence the wavelength distribution of the CHG pulse and also introduces asymmetry in the spectra since it makes the pulse shape of the laser pulse asymmetric.

Studies exploring the spectral and temporal properties of the CHG radiation have been carried out previously at

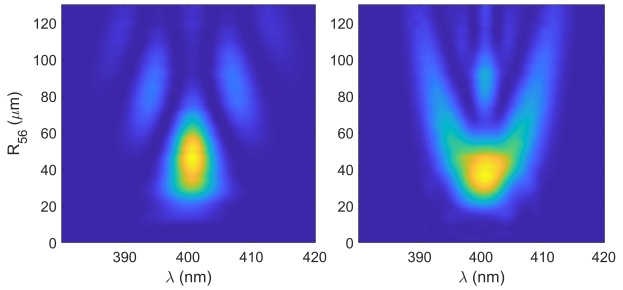

Figure 3: (Left) Simulated CHG spectra for a seed pulse with zero frequency chirp. (Right) Simulated spectra for a seed pulse with strong chirp.

DELTA [6] and similar observations were made at FERMI [7] in the context of HGHG for FELs. In the studies at DELTA, interpreting the CHG spectra was difficult due to the higher-order dispersion present in the seed pulses. In this work, it was attempted to include the effects of higher-order spectral phase on the spectral and temporal properties of the CHG radiation.

THE DELTA SHORT-PULSE SOURCE

At the 1.5 GeV electron storage ring DELTA at TU Dortmund University, a short-pulse facility based on the CHG scheme is being operated to produce ultrashort synchrotron radiation pulses in the vacuum ultraviolet regime [4]. Relevant parameters of the storage ring, the undulators and the laser system are given in Table 1.

Table 1: Parameters of the DELTA Short-Pulse Facility

Storage ring circumference	115.2 m
Electron beam energy	1.5 GeV
Beam current (single-/multibunch)	20/130 mA
Horizontal emittance	15 nm rad
Relative energy spread (rms)	$7{\times}10^{-4}$
Bunch length (FWHM)	80 ps
Modulator/radiator period length	0.25 m
Number of modulator/radiator periods	7
Undulator periods used as chicane	3
Max. modulator/radiator K parameter	10.5
Max. chicane R_{56} (@ 800 A)	~ 170 µm
Laser wavelength	800 nm
Pulse energy @ 800 nm	8 mJ
Min. pulse length	40 fs
Repetition rate	1 kHz

Pulses from a titanium:sapphire laser system are focused directly into the electromagnetic undulator U250 or are frequency-doubled first. The 7 upstream/downstream periods of the U250 act as modulator/radiator for CHG with a chicane between them. A diagnostics beamline is used to observe the spatial and temporal overlap of the laser pulse and the electron bunch with the help of screens and a streak camera. In the dipole magnet downstream, the energy-dependent

ISBN: 978-3-95450-220-2 ISSN: 2673-5474 doi: 10.18429/JACoW-FEL2022-TUP71

path length of the electrons transforms the laser-induced energy modulation to sub-millimeter dip in the longitudinal electron density which results in coherent emission of broadband THz radiation. The laser-electron overlap is then optimized by maximizing the intensity of this THz radiation. On the other hand, laser pulses can be shaped to optimize properties of the THz radiation for experimental purposes, e.g., to produce narrowband radiation to deduce the spectral characteristics of far-infrared detectors [8].

OBSERVATION OF CHG SPECTRA

The spectra of the CHG radiation were recorded using a Czerny-Turner-type spectrometer equipped with an image-intensified CCD (iCCD) camera [9]. With a gating window as short as 2 ns, the iCCD camera allows to capture the CHG spectra without the background of the 2600 spontaneous sychrotron radiation pulses between consecutive CHG pulses. Wavelengths down to 200 nm can be recorded using this method, which covers the 2nd, 3rd and 4th harmonic of the seed wavelength. For observing even shorter wavelengths, an XUV spectrometer was installed recently which can record spectra down to 30 nm [10]. Presently, a MgF window that seperates the beamline from the storage ring vacuum blocks wavelengths below around 130 nm limiting the observation of CHG spectra to the 6th harmonic (133 nm) of the seed wavelength. Shown in Fig. 4 are the observed CHG spectra for the 2nd, 4th and 6th harmonic of the 800 nm seed without (left column) and with (right column) frequency chirp. When seeding with an unchirped laser pulse, pronounced spectral fringes appear at large R_{56}. On the other hand, seeding with a strongly chirped laser pulse results in a parabolic feature similar to the simulations. The asymmetry observed in the spectral features may be attributed to the higher-order dispersion in the seed laser pulse which was not taken into account in Fig. 3.

In order to study the effects of the spectral phase of the seed laser on the CHG radiation, the CHG spectra were simulated for different seed pulse parameters. A convolutional neural network (CNN) [11] was designed using TensorFlow [12] to predict the GDD and TOD from the CHG spectra given as the input. The CNN was trained on a set of over 9000 numerically simulated spectra for different combinations of GDD and TOD. A random noise was added to the simulated spectra in order to account for the noise in the measurements. The spectral phase of the seed pulse was controlled by tuning the separation between the gratings in an optical compressor [13]. The CNN was used to predict the GDD and TOD of the seed pulse from the observed CHG spectra for different grating separations. Figure 5 shows the observed and predicted spectra using the CNN for two different compressor settings.

The trained neural network could reconstruct the spectral features observed for different compressor settings by predicting the GDD and TOD of the seed laser pulse. The mean of the predicted values from 10 trials with the same input and their standard deviation is plotted in Fig. 6. A linear

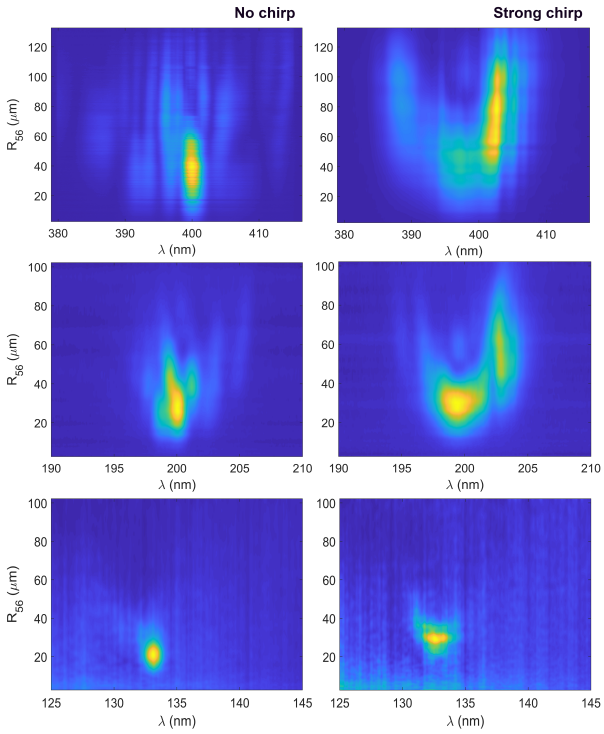

Figure 4: Observed CHG spectra for the 2nd, 4th and 6th harmonic of the seed laser wavelength with unchirped seed pulse (left) and with strong positive chirp (right).

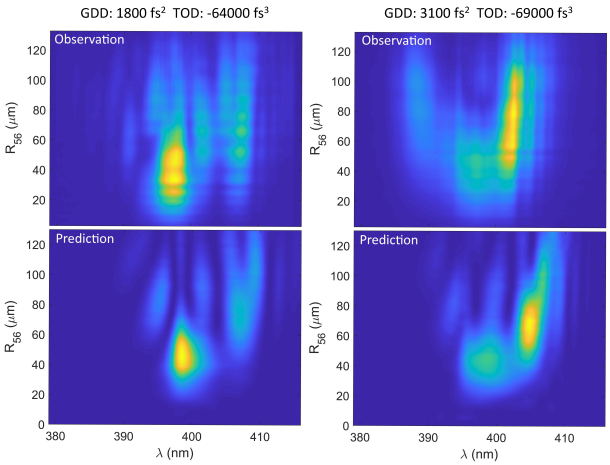

Figure 5: Observed (top) and predicted (bottom) CHG spectra for different settings of the laser compressor at the 2nd harmonic of the seed laser wavelength.

relationship between the grating separation in the compressor and the GDD of the laser pulse was observed (Fig. 6 (top)) while the TOD shows a negative linear relationship to the compressor length (Fig. 6 (bottom)). This behaviour is in agreement with the theory [13]. The results suggest that the asymmetry visible in the spectra could be due to a large negative TOD (> 50000 fs^3) present in the seed laser pulse. The origin of this non-zero TOD could be that the compressor is under-compensating the TOD introduced by

ISBN: 978-3-95450-220-2 ISSN: 2673-5474 doi: 10.18429/JACoW-FEL2022-TUP71

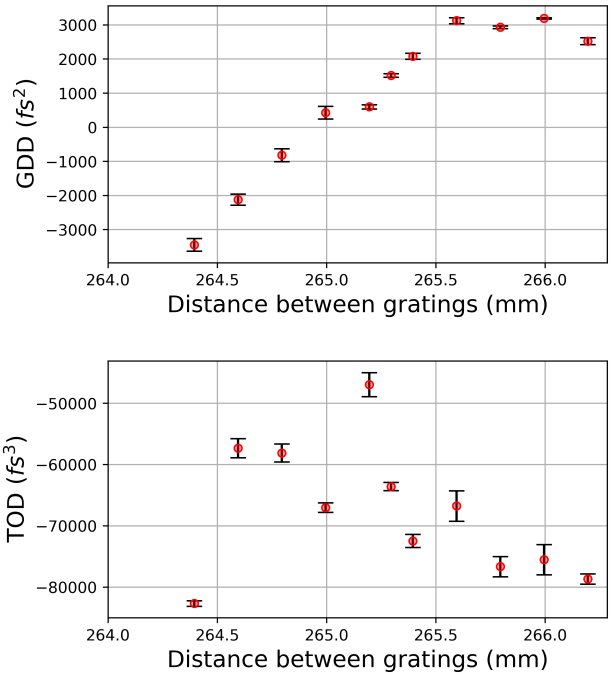

Figure 6: Predicted GDD and TOD values for different compressor settings. The points indicate the mean and the error bars show the standard deviation of predictions from ten individually trained models.

the pulse stretcher in the chirped-pulse amplification scheme. However, it is also to be noted that there are outliers at high GDD which don't fit to the otherwise linear relationship observed. This points to the inefficiency of the model to correctly predict the spectral phase at large GDD values. The CNN model needs to be improved to resolve this. A more detailed study involving direct measurements of the spectral and temporal properties of the seed pulse, such as frequency-resolved optical gating (FROG) [14], is also required to confirm the effects of higher-order dispersion on the CHG spectra. In this study, only the effects of 2nd and 3rd order dispersion on the CHG pulse properties was investigated. Looking into even higher order spectral phase could prove to be helpful in further tailoring the CHG pulses.

CONTROLLING THE SPECTRAL PHASE FOR SHAPING OF THZ PULSES

The control of the spectral phase of the laser pulse was previously implemented using a so-called 4f-pulse shaper setup [15, 16] to optimize the coherently emitted THz pulses. Here, a spatial light modulator (SLM) is used to control individual coefficients of Eq. (4) which allows to correct for TOD introduced by the laser pulse compressor by adding the inverse of the third-order term

$$\varphi_{\mathrm{SLM,corr}}(\omega) = -D_3 \cdot (\omega - \omega_0)^3. \qquad (5)$$

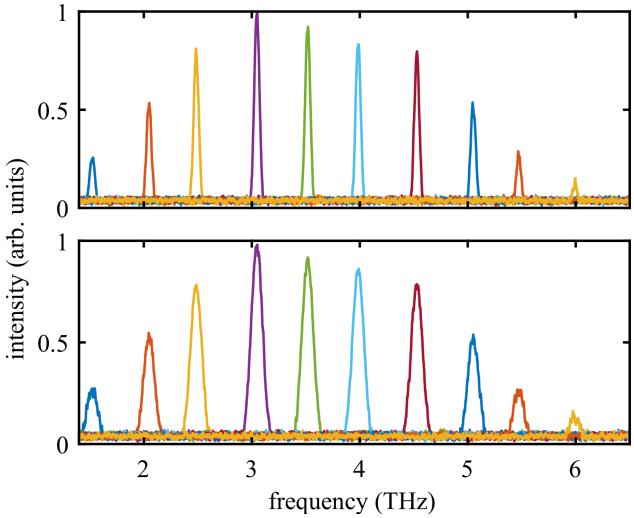

Figure 7: Narrowband THz spectra from a laser-electron interaction with intensity modulation induced by a spatial light modulator. The bandwidth was either set to 80 GHz (top) or 200 GHz (bottom) by changing the phase-shifting pattern.

The correction leads to a linearization of the laser pulse chirp and offers ideal conditions for further control of the pulse shape by a modulation of the spectral phase. Figure 7 shows spectra of coherently emitted, narrowband THz pulses which were generated by adding another modulation of

$$\varphi_{\mathrm{SLM,mod}}(\omega) \propto \cos[\Delta T(\omega - \omega_0)]. \qquad (6)$$

The periodic modulation of the spectral phase causes the occurrence of a pulse train with a temporal spacing of ΔT. Due to the periodic structure, the emission spectra are narrowband and the bandwidth can be controlled by the duration of the pulse train. As the SLM acts as a frequency-dependent phase-shifting filter, further pulse shapes and thus more complex spectral shapes like rectangular spectra can be realized [16].

Currently this method is implemented for long laser pulses with ps length and is successfully demonstrated to be a useful tool in shaping the coherently emitted THz pulses. This way of controlling the spectral phase may also be extended to be used for shaping the CHG pulses as well. For a control over the spectro-temporal properties of sub-ps CHG pulses, however, the intensities could exceed the damage threshold of the SLM. Methods to avoid this problem are currently under investigation.

ACKNOWLEDGEMENTS

We are pleased to thank our colleagues at DELTA and the TU Dortmund University. The continuous support from other institutes, particularly from DESY Hamburg, HZB Berlin, and KIT Karlsruhe is gratefully acknowledged.

ISBN: 978-3-95450-220-2 ISSN: 2673-5474 doi: 10.18429/JACoW-FEL2022-TUP71

REFERENCES

[1] R. Coisson and F. De Martini, "Free-electron coherent relativistic scatterer for UV-generation", *Physics of Quantum Electronics*, vol. 9, pp. 939-960, 1982.

[2] M. Labat *et al.*, "Coherent harmonic generation on UVSOR-II storage ring", *Eur. Phys. J. D*, vol. 44, pp. 187-200, 2007. doi:10.1140/epjd/e2007-00177-6

[3] G. De Ninno *et al.*, "Generation of Ultrashort Coherent Vacuum Ultraviolet Pulses Using Electron Storage Rings: A New Bright Light Source for Experiments", *Phys. Rev. Lett.*, vol. 101, p. 053902, 2008. doi:10.1103/PhysRevLett.101.053902

[4] S. Khan *et al.*, "Generation of ultrashort and coherent synchrotron radiation pulses at DELTA", *Sync. Rad. News*, vol. 26, no. 3, p. 25, 2013. doi:10.1080/08940886.2013.791213

[5] G. Stupakov, "Using the beam-echo effect for generation of short-wavelength radiation", *Phys. Rev. Lett.*, vol. 102, p. 074801, 2009. doi:10.1103/PhysRevLett.102.074801

[6] M. Huck *et al.*, "Ultrashort and Coherent Radiation for Pump-probe Experiments at the DELTA Storage Ring", in *Proc. IPAC'14*, Dresden, Germany, Jun. 2014, pp. 1848–1851. doi:10.18429/JACoW-IPAC2014-WEOAA03

[7] D. Gauthier *et al.*, "Spectrotemporal Shaping of Seeded Free-Electron Laser Pulses", *Phys. Rev. Lett.*, vol. 115, p. 114801, 2015. doi:10.1103/PhysRevLett.115.114801

[8] C. Mai, M. Brosi, B. Büsing, F. Frei, C. Gerth, S. Khan, *et al.*, "A Tunable Narrowband Source in the Sub-THz and THz Range at DELTA", in *Proc. IPAC'18*, Vancouver, BC, Canada, Apr. 4, pp. 4534–4537, doi:10.18429/JACoW-IPAC2018-THPMK098

[9] Andor iStar DH334T 18U-E3, https://andor.oxinst.com/products/intensified-camera-series/istar-334t

[10] HP Spectroscopy easyLIGHT XUV, https://www.hp-spectroscopy.com/easylight-xuv

[11] Y. LeCun, Y. Bengio, and G. Hinton, "Deep learning", *Nature*, vol. 521, p. 436, 2015. doi:10.1038/nature14539

[12] M. Abadi *et. al.*, "Tensorflow: A system for large-scale machine learning", *12th USENIX Symposium on Operating Systems Design and Implementation*, 265, 2016.

[13] P. Ungelenk *et. al.*, "Continuously tunable narrowband pulses in the THz gap from laser-modulated electron bunches in a storage ring", *Phys. Rev. ST Accel. Beams*, vol. 20, p. 020706, 2017. doi:10.1103/PhysRevAccelBeams.20.020706

[14] R. Trebino *et. al.*, "Measuring ultrashort laser pulses in the time-frequency domain using frequency-resolved optical gating", *Rev. Sci. Instrum.*, vol. 68, no. 9, p. 3277, 1997. doi:10.1063/1.1148286

[15] A. M. Weiner, "Femtosecond pulse shaping using spatial light modulators", *Rev. Sci. Instrum.*, vol. 71, pp. 1929–1960, 2000. doi:10.1063/1.1150614

[16] C. Mai, "Towards arbitary Pulse Shapes in the Terahertz Domain", C. Mai, B. Büsing, A. Held, S. Khan, and D. Krieg, "Towards Arbitrary Pulse Shapes in the Terahertz Domain", in *Proc. IPAC'21*, Campinas, Brazil, May 2021, pp. 3977–3979. doi:10.18429/JACoW-IPAC2021-THPAB097